POLITECNICO DI TORINO
Repository ISTITUZIONALE

3D-printed antibacterial filters obtained via digital light processing exploiting surface microwaves functionalization with natural amino acids

Original
3D-printed antibacterial filters obtained via digital light processing exploiting surface microwaves functionalization with natural amino acids / D'Aloia, M., Cue López, R., Villata, S., Vasile, N.S., Martínez Campos, E., Montalvillo Jiménez, L., Pirri, C.F., Frascella, F., Bosch, P., Roppolo, I.. - In: APPLIED MATERIALS TODAY. - ISSN 2352-9407. - 44:(2025), pp. 1-12. [10.1016/j.apmt.2025.102779]

Availability:
This version is available at: 11583/3017522 since: 2026-11-04T15:45:54Z

Publisher:
Elsevier

Published
DOI:10.1016/j.apmt.2025.102779

Terms of use:

This article is made available under terms and conditions as specified in the corresponding bibliographic description in the repository

Publisher copyright

(Article begins on next page)

13 November 2026

Applied Materials Today 44 (2025) 102779

Contents lists available at ScienceDirect

Applied Materials Today

journal homepage: www.elsevier.com/locate/apmt

3D-printed antibacterial filters obtained via digital light processing exploiting surface microwaves functionalization with natural amino acids

Maria D'Aloia [a,b,c], Raquel Cue López [a,c], Simona Villata [a,c], Nicolò Santi Vasile [d,e], Enrique Martínez Campos [f], Laura Montalvillo Jiménez [g], Candido Fabrizio Pirri [a,c,d], Francesca Frascella [a,d], Paula Bosch [g], Ignazio Roppolo [a,c,d,*]

[a] Department of Applied Science and Technology, Politecnico di Torino, Corso Duca degli Abruzzi 24, 10129 Turin, Italy
[b] Department of Chemistry, Biology and Biotechnology, University of Perugia, Via Elce di Sotto 8, 06123 Perugia, Italy
[c] PoliTOBioMEDLab, Politecnico di Torino, Corso Duca degli Abruzzi 24, Torino, 10129, Italy
[d] Center for Sustainable Future Technologies, Italian Institute of Technology, Via Livorno 60, 10144 Turin, Italy
[e] Department of Environment, Land and Infrastructure Engineering, Politecnico di Torino, Corso Duca degli Abruzzi 24, Turin, 10129, Italy
[f] Grupo de Síntesis Orgánica y Bioevaluación, Instituto Pluridisciplinar (UCM), Unidad Asociada al Instituto de Ciencia y Tecnología de Polímeros, Instituto de Química Médica (CSIC), Paseo de Juan XXIII 1, 28040 Madrid, Spain
[g] Departamento de Química Macromolecular Aplicada, Instituto de Ciencia y Tecnología de Polímeros, Consejo Superior de Investigaciones Científicas (CSIC), C/Juan de la Cierva 3, 28006 Madrid, Spain

ARTICLE INFO

Keywords:
3D printing
Antibacteric
Filters
CFD design
Amino acids functional

ABSTRACT

3D printing based on Digital Light Processing (DLP) technology was used to develop antibacterial filters, combining design versatility and manufacturing precision. The advantages of 3D printing, including the ability to produce complex geometries, reduction of material waste, and rapid iteration between design and production, were exploited to make two different filter configurations. In addition, these geometries were analyzed by computational fluid dynamics (CFD) to evaluate and compare their effectiveness in terms of flow distribution and antibacterial potential. The filters were successfully printed using photosensitive resins based on polyethylene glycol diacrylate (PEGDA), acrylic acid (AA) and glycidyl methacrylate (GMA). Subsequently, they were subjected to functionalization processes that employed various chemical techniques and functional molecules, notably arginine and agmatine, which antibacterial activity has been widely demonstrated. These processes enabled the incorporation of specific groups aimed at bacterial adhesion and inactivation. Characterization of the degree of functionalization was conducted by spectroscopic and microscopic techniques, confirming the effectiveness of the surface treatment. Finally, the filters were tested against Gram-positive and Gram-negative bacteria to evaluate their antibacterial efficacy. Results showed a significant reduction in bacterial viability for agmatine-functionalized PEGDA/GMA-based filters, demonstrating that both filter design and functionalization play a crucial role in achieving high antibacterial performance. The results for the other filters, however, were uncertain, and further analysis will be needed.

This study, however, confirms the potential of DLP technology, which, together with appropriate functionalization methods, suggests new possibilities for the development of customizable and functional devices.

Introduction

In recent years, air pollution has become a serious threat to the environment and human health [1]. The problem arises from various sources, including natural processes and human activities, with the release of harmful gases and solid particulate matter. Particulate substances include solid particles, liquid droplets, or mixtures of both, including aerosols formed with viruses, bacteria, pollen, fungi, spores, and allergen [2], which may lead to allergic reactions and respiratory diseases [3]. Air is also a vehicle for infectious diseases such as the Avian flu and the recent COVID-19 pandemic [4–7], and prolonged exposure to air pollutants can cause respiratory problems like asthma and lung cancer, as well as cardiovascular issues [8], with about seven million premature death each year according to WHO [9].

In this context, effective air filtration systems are crucial [1], as evidenced by the recent COVID-19 pandemic, which emphasized the

* Corresponding author.

https://doi.org/10.1016/j.apmt.2025.102779
Received 13 February 2025; Received in revised form 24 April 2025; Accepted 7 May 2025
Available online 17 May 2025
2352-9407/© 2025 The Author(s). Published by Elsevier Ltd. This is an open access article under the CC BY-NC-ND license (http://creativecommons.org/licenses/by-nc-nd/4.0/).

importance of effective filters, not only in face masks but also in ventilation systems for enclosed spaces [10]. Therefore, there is a growing demand for sustainable, multifunctional filter materials with high filtration performance [3,11]. The sustainability of filters must be evaluated not only in the choice of materials and manufacturing techniques, but also in the design of their geometry, which affects aerodynamic resistance and, consequently, factors such as acoustic and thermal impact and energy consumption [12].

Effective filtration can be achieved by optimizing structural and chemical properties of filters, such as pore size, surface charge, hydrophilicity, specific surface area, and mechanical stability[13]. Most air filters are made of polymeric materials [13], e.g. polyacrylonitrile (PAN), polyurethane (PU), polylactide, nylon-6, polyimide (PI), polysulfone (PSF), and others [10,14–18], in the form of nanofibrous structures or porous membranes [10], typically processed through include electrospinning [1,3,10,13,16–19]. This technique allows for structures with high specific surface area and small pore size [19], but even though many studies have reported the effectiveness of electrospinning [10,19,20], it has limitations in terms of throughput and mechanical stability, often requiring additional support materials, e.g., fabric, plastic or metal mesh [10,19]. Therefore, new manufacturing techniques are needed to overcome these limitations.

Recently, additive manufacturing (AM) techniques, or 3D printing, have emerged as alternatives to or complements to electrospinning [19], offering advantages such as speed, sustainability, flexibility and low costs These techniques enable the design and fabrication of structures with precise internal and external geometries, reducing material waste, especially if compared to traditional subtractive manufacturing processes [21–24]. In addition, advances in polymer chemistry for AM are promoting the use of biodegradable and recyclable polymers, promoting sustainability and circular economy [23,25]. Finally, AM can be adapted to consume less energy, especially in applications where traditional manufacturing processes require extensive processing or multiple steps; the ability to produce complex geometries in a single step, in fact, reduces manufacturing energy consumption [23,25].

In the area of filtration, additive manufacturing allows the optimization of the chemical and structural properties of filters [13], improving their effectiveness and allowing the incorporation of antimicrobial properties [12]. Many studies show the benefits that 3D printed antibacterial products could have [26].

However, the choice of materials is crucial, as antimicrobial activity can result from geometry, the material itself, or post-printing functionalization processes. These processes must be carefully selected to avoid damage to the printed geometries.

Antibacterial surfaces can act according to two mechanisms, depending on whether their effect is based on the release of bactericidal agents or on surface-bacteria contact [27]. Release-based systems incorporate bactericidal substances, such as silver nanoparticles (AgNPs) or antibiotics, which are released gradually to kill nearby bacteria [27]. For example, silver nanoparticles (AgNPs) as powerful broad-spectrum antibacterial characteristics have been widely used to prepare antibacterial coatings based on the release of bactericidal mechanisms [27]. Contact-killing surfaces, on the other hand, are functionalized with antibacterial agents that eliminate bacteria by adhesion, exploiting chemical or physical interactions [27]. The mechanism of bacterial adhesion is very complex, and it is influenced by several factors [28], including the surface chemistry of both the substrate and the bacterium itself, as well as the surrounding environment and conditions. Most molecules used in this context exploit their positive charges to disrupt the bacterial membrane or to inhibit the normal metabolic activities of bacterial cells [27].

Recently, attention has also been turned to new techniques involving functionalization with antimicrobial polymers and antimicrobial peptides (AMPs) [29,30]; among those two categories it can be mentioned polyethylenimine (PEI), chitosan [31], or peptides with a positive charge and a large number of hydrophobic residues, like those rich in arginine or glycine [31]. They act by destroying bacterial membranes through electrostatic interactions and, unlike traditional antibiotics, these agents do not cause resistance and show more efficient and broad-spectrum action [32].

Focusing on anti-bacteric filtration systems produced by 3D printing, McFarland et al. (2022) applied a coating by electrodeposition onto the surface of halysite nanotubes (HNTs) with metals (copper, silver and zinc), which are known to possess potent antiviral and antimicrobial properties. The metal-coated HNTs (mHNTs) were then added to polylactic acid (PLA) and 3D printed by extrusion to form a filter for face masks [33]. Another recent work developed a chitosan-graphene oxide-silver (CS-GO-AgNP) composite membrane with effective bacterial trapping action in aqueous environments [34]. Some natural molecules are also effective in giving antibacterial properties: for example, in 2021, Thavornyutikarn and coworkers developed new antibacterial composite filaments for three-dimensional (3D) FFF (Fused Filament Fabrication) printing based on thermoplastic polyurethane (TPU) enriched with green tea (GT) and tannic acid (TA), both natural substances with antibacterial properties [35]. Lehnen et al. recently designed filter devices with adjustable surface functionalization effective in antibacterial water filtration [36].

This study aims to combine the versatility and sustainability of 3D printing with functionalization techniques to create complex-shaped filters with antibacterial properties. Among 3D printing methods, Vat-Photopolymerization (VP) offers high resolution and affordable material and equipment costs. They are based on the spatially controlled solidification, layer-by-layer, of photosensitive liquid resins [37] by a programmable light source controlled by software; the light emission can be controlled in terms of intensity, field distribution, and wavelength [38]. In VP techniques there is no need for support material, as the uncured material itself acts as a support [39]. Moreover, there are fewer limitations on the viscosity range suitable for the fabrication process, but the material choices are limited to liquid or soluble photopolymers, which might be a disadvantage [40]. Among VP technologies, Digital Light Processing (DLP) is of particular interest due to its speed and resolution, enabling the creation of structures that possess a level of complexity so to reduce microorganism flow [40,41]. Here, filters design was tested with Computational Fluid Dynamics (CFD) modelling, which are useful for predicting the effectiveness of different geometric configurations without expensive physical experiments [42]. By leveraging CFD simulations, researchers can efficiently investigate the interplay between filter morphology, flow patterns, and filtration efficiency, enabling the design of filters that optimize particle capture while minimizing pressure drops [43,44]. Selected studies highlight the importance of integrating CFD models with targeted experiments to validate simulations and further refine filter designs, highlighting the potential of CFD simulations to accelerate the development of high-performance filtration solutions while reducing associated time and costs [45–48].

In this work, DLP technology allows the chemical properties of the material to be controlled [49,50] by incorporating functional monomers for surface-exposed groups as anchor points for functionalization. Surface functionalization strategy exploits AMPs mechanism to impart antibacterial properties, specifically by grafting amine groups onto the surface, since the antibacterial role of amines has been extensively studied [51–56]. This method offers superior advantages, as the antimicrobial agent is covalently bound to the device, providing a more stable and long-lasting action against microbes [57]. To this aim, arginine, a natural, hydrophilic amino acid with a large guanidinium cationic group, and agmatine, a primary amine formed by decarboxylation of arginine were exploited [58]. The antimicrobial activity of arginine (AR), due to the guanidinium group, has been widely demonstrated [59–64], and since their structure is similar, we will try to demonstrate the efficacy of agmatine (AG) as well. These molecules, used also in the biotechnology, pharmaceutical, and food industries, offer a sustainable option, since they can be derived from industrial

waste or by-product [65–67].

Two acrylate/epoxy formulations, based on polyethylene glycol diacrylate (PEGDA), acrylic acid (AA) and glycidyl methacrylate (GMA), are prepared and processed using a digital light processing (DLP)-3D printing technique. $PEGDA_{250}$ is selected as structural monomer because of its low molecular weight, that assures dimensional stability, high degree of crosslinking, and good printability. The acrylate groups in its structure promote a radical polymerization [68]. Acrylic acid (AA) and glycidyl methacrylate (GMA) monomers were chosen to incorporate reactive functional groups (carboxylic and epoxy groups, respectively) into the polymeric structures by copolymerization with $PEGDA_{250}$ during the 3D printing step [69]. Arginine and agmatine were bonded exploiting the reactive primary amino group present in both molecules [70].

Related to functionalization methods, two techniques were tested: conventional heating (CH) and microwave-assisted (MW) functionalization. Thermally activated chemical reactions are standard and effective but generate temperature gradients [71] and need long timescales, consuming energy due to dependence on convection currents and thermal conductivity [72,73]. In addition, the formation of thermal gradients can lead to non-uniform transformations, creating obstacles to scale production [71]. In contrast, microwave-assisted reactions are based on the conversion of electromagnetic energy into thermal energy [72]. Microwave energy easily penetrates the material, which can be homogeneously heated rapidly and all at once, resulting in volumetric heating [74]. This occurs due to rotational and vibrational effects, thus reducing thermal gradients and preventing sample damage. MW technology also allows the use of environmentally friendly solvents, resulting in cleaner products [71]. MW strategies provide an alternative heat source and have given the possibility of reducing reaction times to the order of seconds or minutes, versus hours or days in CH strategies. Additionally, the high product yield, high product purity and high reproducibility of MW-assisted reactions make this technique green and highly desirable synthetic strategy [71].

Experimental analyses are conducted to optimize procedures, considering the compromise between surface functionalization, reaction time, and final sample properties. Finally, the antibacterial properties of the functionalized filters are evaluated against *Escherichia coli* and *Staphylococcus aureus* bacteria.

Materials and methods

Materials

Poly(ethylene glycol)diacrylate ($PEGDA_{250}$, Mn = 250 g/mol), acrylic acid (AA, 99 %, Mn = 72.063 g/mol) and glycidyl methacrylate (GMA, 97 %, Mn = 142.15 g/mol) were purchased from Sigma-Aldrich (Merck Company, Darmstadt, Germany) and used as received. As a photoinitiator, phenylbis (2,4,6-trimethylbenzoyl) phosphine oxide (BAPO, 97 %) was used; brilliant green dye (BG, dye content ~90 %) was used in some of the formulations. Both BAPO and BG were purchased from Sigma-Aldrich (Merck Company, Darmstadt, Germany) and used as received. Ethanol (EtOH, 99.8 %) was used for washing and sonication steps. As grafting agents in functionalization, arginine (L-arginine, 98 %) and agmatine (agmatine sulfate, 97 %), were used. In some of the reactions, EDC/NHS (1-ethyl-3-(3-dimethylaminopropyl) carbodiimide / *N*-hydroxy-succinimide) were used as coupling agents. Agmatine was purchased from Alfa Aesar (Thermo Fisher Scientific, USA); arginine, EDC and NHS were purchased from Sigma-Aldrich (Merck Company, Darmstadt, Germany). Buffers used were PBS and Tris–HCl (Merck), Milli-Q water was used as solvent. All the products were used as received.

Geometry study and flow simulation

Two filter-type structures were designed: the first geometry (configuration A) involves the superposition of several equal layers, rotated with respect to each other; this filter operates in a predominantly axial direction and is ineffective with radial or circumferential air flows. Filters with this geometry were 3D printed in two different sizes: smaller (1.5 cm in diameter and 2 mm thick) and larger (3 cm diameter and 1.5 cm thickness). The second geometry (configuration B) is more complicated and can also filter radial or circumferential flows; a series of concentric perforated walls are used for this purpose. In the axial direction, the same principle as above is used, that is, a series of layers of equal geometry that are offset from each other. These layers also have the function of holding the walls together. Filters with this geometry were 3D printed (1.5 cm in diameter and 2 mm in thickness and 3 cm in diameter and 4 cm in height). CADs of the different geometries are shown in Fig. 1A.

Computational model description

CFD simulations can provide useful data on filter performance, highlighting velocity profiles, pressure losses and particle trajectories in 1D to 3D configurations. These results help predict and optimize filter performance by guiding filter design. In our study, simulations were conducted with COMSOL Multiphysics, a versatile platform for modeling and analyzing complex physical phenomena that is ideal for studying filtration systems because of its capabilities in thermo-fluid dynamics and particle motion. We integrated key physical phenomena, such as thermo-fluid dynamics of turbulent flows and particle tracking, into our models to analyze the complex interactions between flow and particles in the filter matrix.

Using COMSOL Multiphysics, two filter configurations (A and B) were simulated in a cylindrical tube with three thicknesses (1, 2 and 4 layers), examining fluid dynamics and particle interactions to evaluate the impact of filter density on characteristics such as residence time and pressure losses. The simulations assumed a cylindrical tube with the filter positioned inside, through which a liquid containing bacterial particles was fed. Each filter thickness was tested under five different flow rates, ranging from 0.1 ml/min to 1000 ml/min, to capture a broad spectrum of operational demands. In addition to fluid flow analysis, particle tracing was incorporated to simulate bacterial contamination, modeling the microorganisms as spherical particles dispersed within a liquid phase. This setup allowed for the evaluation of particle trajectories, wall interactions, and velocity profiles under various flow intensities, reflecting how each configuration responds to typical challenges in filtration scenarios. A summary of the simulated conditions, including the liquid composition (water with a bacterial density at an optical density of 0.01), the outlet working pressure (atmospheric), and specific flow rates, is presented in Table S1.

We used the Navier-Stokes equations to govern the fluid flow, capturing the momentum, velocity, and pressure fields of the air moving through the filter. Additionally, the k-epsilon turbulence model was employed to provide a detailed description of turbulence by calculating turbulent kinetic energy and its dissipation rate, which are pivotal for predicting the flow behavior in the filter's intricate geometrical configurations. An energy balance equation was also integrated into our simulations to account for any thermal effects, ensuring that temperature variations do not adversely affect the overall filtration performance.

Particle tracking equations were used to simulate the trajectory of bacterial particles through the filter, evaluating their interactions with the filter material and the efficiency of the system. The model assumes that the particles are spherical, with mass and density derived from experimental data, and that their motion is related to fluid dynamic calculations.

The particle trajectory and physical properties in the model are determined by the particle tracing module for the fluid flow interface in Comsol. In this module, the motion, the particle momentum, the drag and gravity force, the particle velocity and its trajectory, the particle-particle and particle-walls interactions are determined by solving the

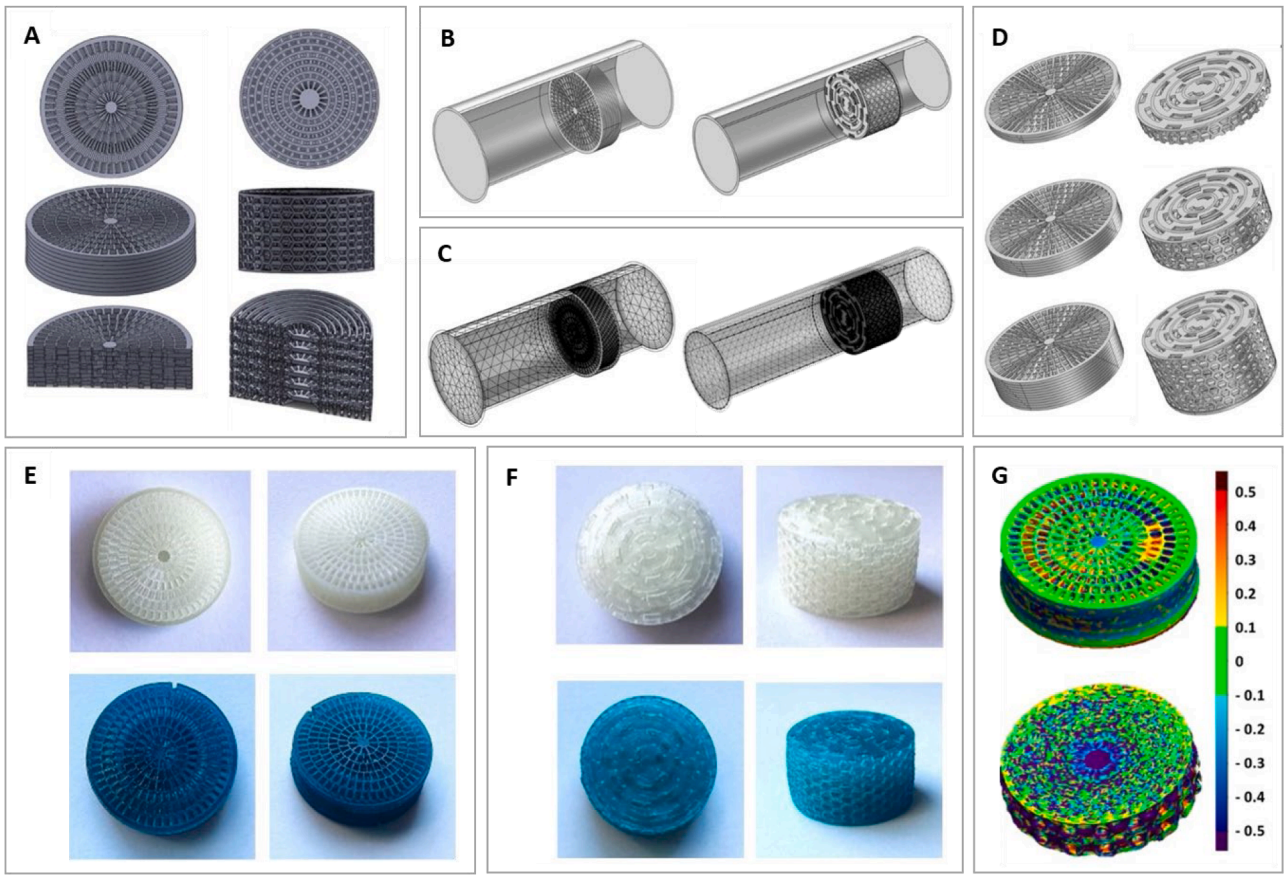


Fig. 1. Overview and analysis of two 3D printed filter configurations: Configuration A: CAD model of configuration A (on the left) and B (on the right (A). Simulated fluidic domain containing filters inside a cylindrical tube (configuration A on the left; configuration B on the right) (B). Finite element mesh for configuration A (on the left) and configuration B (on the right) (C). Filters configuration with varying thicknesses: configuration A on the left (φ35mm - 1 layer (2.4 mm), 2 layers (4.8 mm), and 4 layers (9.6 mm)); configuration B on the right (φ25mm - 1 layer (3 mm), 2 layers (6 mm), and 4 layers (12 mm)) (D). Configuration A 3D printed samples (φ35mm; h15mm) using PEGDA/AA (top row) and PEGDA/GMA (bottom row) (E). Configuration B 3D printed samples (φ25mm; h30mm) using PEGDA/AA (top row) and PEGDA/GMA (bottom row) (F). Evaluation of fidelity between the printed filters and CAD models using 3D scanning (top: configuration A, bottom: configuration B) (G).

differential equations listed in Table S2. These detailed equations make it possible to analyze complex interactions between flow and particles, optimizing filter design. Table S2 reports key equations used in our simulations. The quality of the mesh is crucial for ensuring convergence and accuracy of the results. Our models used a mesh consisting of $3e^6$ to $5e^6$ tetrahedral elements, ensuring adequate resolution to represent the phenomena in the filter in detail.

Formulation preparation

Two photocurable formulations were prepared with different weight ratios between monomers (Table 1). Each solution is prepared in a black falcon to avoid polymerization due to visible light. The solution is then sonicated for a few minutes to make it homogeneous.

Each formulation was prepared by mixing the monomers first and then adding 2 wt% of BAPO as photoinitiator. PEGDA/GMA-based structures need a dye to improve printing resolution: 0.01 wt% of brilliant green (BG) is added to the solution, which was then stirred mechanically at 40 °C to make the dye dissolve completely.

3D. Printing

As 3D printing equipment, a Pico 2 HD DLP-3D printer (Asiga, Australia) was used. This 3D printer has a LED light source with a wavelength of 405 nm, build area of 64 × 40 × 76 mm^3 with nominal XY resolution of 50 μm, and minimum Z-axis control of 1 μm. All CAD designs were produced with Solidworks program and exported in STL format. The printing process was performed with a 200 μm layer thickness, an approach and separation velocity of 0.5 mm/min, a slider velocity of 1 mm/min, and 5 s wait time after each step. Light intensity, exposure time and heating temperature were different for each formulation and are shown in Table 1. After printing, the samples were washed in ethanol to remove the residual resin. Objects were then post-cured to complete the polymerization and to strengthen the objects. Post-curing was performed in a UV chamber lamp (Asiga Flash or RobotFactory UV oven) for 3 min. For the optimization of surface modification reactions, flat strips of size 1 × 5 cm and thickness of 600 μm were 3D printed.

Table 1
– Composition of each formulation and 3D printing settings (200 μm of slicing thickness).

Formulation	Composition	Dye (phr)	Exposure time (s/layer)	Initial exposure time (s/layer)	Light intensity (mW/cm2)	Temperature (°C)
PEGDA/AA	PEGDA:AA = 80:20	–	1	2	25	25
PEGDA/GMA	PEGDA:GMA = 80:20	0.1	5	7	35	30

Functionalization

Different surface functionalization methods (conventional heating and microwave heating) were exploited. At the end of each reaction, samples are exhaustively washed with water, dried with absorbent paper and placed in a vacuum desiccator at −70 cmHg, for at least 6 hours at room temperature.

Conventional heating

The general procedure for surface modification through conventional reaction is the following: the solid reactants are placed in a round-bottom flask provided with a magnetic stirrer and a refrigerator, together with a sufficient volume of the specific buffer solution. The 3D printed specimen is added in the solution, and the reaction is maintained under flex for the selected time with the aid of a sand bath (see all conditions in Table 2 and Table 3).

Microwave-assisted surface modification

Microwave reactions are performed in an Anton-Paar Monowave 300 reactor. A 10 mL borosilicate glass vial sealed with silicon septum, with an operation volume of 2–6 mL (G10 vial), is used. Reactions are carried out at 150 °C for 3, 5 and 7 min (see all conditions in Table 2 and 3).

Characterization

3D. Scanner

A 3D scanner was used to compare the printed geometry with the one drawn on CAD software and thus be able to evaluate the printing fidelity. The scanner used is the 3Shape E4 (3Shape A/S, Copenhagen, Denmark), equipped with four 5 MP cameras and with a measurement accuracy of 4 μm. Scan analysis was performed with Convince Software from 3Shape. The sample Is covered with a thin layer of talc and placed on the scanner platform. The resulting image is compared with the original CAD file to obtain a colorimetric map.

FTIR spectroscopy

The IR spectra were recorded with a PerkinElmer Spectrum Two spectrometer in transmission mode, with a resolution of 4 cm^{-1}, in a wavenumbers range of 400 – 4000 cm^{-1}. The obtained spectra were referenced at Abs_{4000}=0, so that all the spectra have the same baseline. The spectra were normalized with respect to the 1720 cm^{-1} peak, corresponding to the ester group.

Contact angle measurement

Water contact angle was determined using a CAM200 goniometer (KSV instruments), equipped with a video camera and an image analyzer. The tests were performed at room temperature using the sessile drop technique. A 3 μL droplet of water (72,8 Mn/m) was placed onto the sample surface, and the static angle was measured. The test was repeated ten times for each sample.

TGA

TGA Q500 thermal analyzer (TA instruments, New Castle, DE, USA) was used to perform thermogravimetric measurements under dynamic mode using air atmosphere. Samples were heated from room temperature to 800 °C at a heating rate of 10 °C/min. The initial degradation temperature (T_0) was obtained at 5 % of mass loss and temperature at the maximum degradation rate (T_{MAX}) were obtained from the first derivative of the TGA curves (DTG).

EDX

The distribution of nitrogen on surface of modified materials is evaluated by Scanning Electron Microscopy (SEM) with Energy Dispersive X-Ray Analysis (EDX). A Bruker Nano equipment with Xflash Detector 5030 was used to investigate the relative concentration of nitrogen retained on the unreacted and modified coating surface after the different reaction processes. A probe current of 2.0×10^{-9} A and an accelerating voltage of 15 Kv were used. The spot size irradiated was approximately 0.5 mm2 for all specimens. To determine the relative nitrogen concentrations on the membrane surface, X-ray net counts were obtained at three random locations for each specimen with a collection time of 30 s. Three specimens were used for each condition. Samples were metalized with Cr prior to being analyzed. From all samples, an X-ray map was obtained showing the distribution of nitrogen along the entire surface.

Swelling test

The study for swelling of 3D-printed samples was carried out to verify the maximum amount of water the sample is able to retain. The samples were immersed in 25 mL of water for 24 hours at room temperature. Swelling percentage (ws%) in water was determined by measuring the weight difference between the swelled sample (W_w) and the initial one (W_i).

$$ws\% = \left(\frac{W_w - W_i}{W_i}\right)\cdot 100$$

After the swelling test, a recovery test was performed to evaluate the effectiveness of the drying procedure. Samples were weighed after a period of 24 h immersed in water; afterwards, they were placed in a vacuum pump for 6 h and weighted again (W_f); the difference between these two values gives the percentage of recovery (wr%).

$$wr\% = 100 - \left[\left(\frac{W_f - W_i}{W_i}\right)\cdot 100\right]$$

Bacterial seeding

Samples were first sterilized in a 48-well plate, using two initial washes with 1 mL of EtOH 70 %. Subsequently, surfaces were exposed to 60 min of UV light before a final wash with PBS. For bacteria inoculum, 1:10 dilutions of previously obtained 0.8 O.D. bacterial suspensions (*Staphylococcus aureus* and *E. coli*) stored at 4 °C were prepared in LB media and left at 37 °C under constant shaking of 125 rpm for 18–24 h. Next, it was verified that the optical density of bacteria cultures was 0.8 at 600 nm using a spectrophotometer (Hach, USA) previous to cell seeding over the samples.

Then, 1 mL of this inoculum was added to each sample and incubated for 24 h at 37 °C. Finally, LIVE/DEAD™ BacLight™ (ThermoFisher

Table 2
Experimental conditions for surface functionalization.

Matrix	Functional molecule	Coupling agent	Buffer	pH	Treatment	Name
PEGDA/AA	Arginine (15.1 mg/mL)	EDC (5.4 mg/mL) NHS (3.9 mg/mL)	Phosphate buffer (PBS)	5.8	Conventional heating	PAA-AR-C
					Microwave heating	PAA-AR-M
	Agmatine (19.7 mg/mL)	—	Tris–HCl	8.6	Conventional heating	PAA-AG-C
					Microwave heating	PAA-AG-M
PEGDA/GMA	Arginine (15.1 mg/mL)	—	Tris–HCl	8.6	Conventional heating	PGMA-AR-C
					Microwave heating	PGMA-AR-M
	Agmatine (19.7 mg/mL)	—	Tris–HCl	8.6	Conventional heating	PGMA-AG-C
					Microwave heating	PGMA-AG-M

Table 3
– Optimized reaction parameters.

Name	Matrix	Functionalization molecule	Treatment	Optimized Conditions	Type pf reaction
PAA-AR-C	PEGDA/AA	Arginine	Conventional heating	100 °C, 70 rpm, 24h	Michael addition + Amidation
PAA-AR-M		Arginine	Microwave heating	150 °C, 5min	
PAA-AG-C		Agmatine	Conventional heating	100 °C, 70 rpm, 24h	
PAA-AG-M		Agmatine	Microwave heating	150 °C, 7min	
PGMA-AR-C	PEGDA/GMA	Arginine	Conventional heating	100 °C, 70 rpm, 24h	Michael addition + Epoxy opening
PGMA-AR-M		Arginine	Microwave heating	150 °C, 3min	
PGMA-AG-C		Agmatine	Conventional heating	100 °C, 70 rpm, 48h	
PGMA-AG-M		Agmatine	Microwave heating	150 °C, 7min	

Scientific, USA) kit test was used to evaluate biofilm formation and viability. Staining was performed for 15 min in dark conditions at room temperature, followed by rinsing twice with PBS. This assay analyzes the membrane integrity of the cell, staining green (SYTO® 9) if they are intact, or red (Propidium Iodide) if the membrane is compromised.

The fluorescence signals were detected using an Eclipse Ti2 Nikon (Tokyo, Japan) microscope equipped with a Crest X-Light spinning disk. Images were acquired by triplicate, and live and dead bacterial cells were quantified using ImageJ software. Fluorescence-stained images, acquired in triplicate, were converted to 8-bit grayscale format (*Image > Type > 8-bit*) to standardize the data for analysis. To differentiate live and dead bacteria, thresholding was applied (*Image > Adjust > Threshold*) to isolate the fluorescent signals corresponding to each population. The threshold levels were adjusted to ensure accurate segmentation of the regions of interest (ROIs). Following this, the *Analyze > Measure* function was used to calculate the mean fluorescence intensity and the total area of the detected ROIs, which correlate with the abundance of live or dead bacteria. This process was repeated for all triplicate images, and the average values were used to quantify the live-to-dead ratio of bacterial cells. Statistical analysis was performed with two-ways ANOVA (* $p < 0.05$, ** $p < 0.01$, *** $p < 0.001$, ****$p < 0.0001$).

Results

In the realm of enhancing the performance of 3D printed filters, CFD modeling emerges as a key tool, allowing the interaction between filter morphology, flow, and filtration efficiency to be explored. This optimizes filter design, reducing pressure drops and speeding up the design process, reducing time and cost.

The two geometric configurations, A and B, are designed to create distinct fluidic pathways (Fig. 1B and C). This design aspect influences the residence time of particles within the filter, the number of particle-wall collisions, and the overall particle retention efficiency. The various geometries simulated are illustrated in Fig. 1D, with different thicknesses tested for both the configuration.

The study evaluated filter performance by varying flow, showing how geometry affects filtration characteristics. The analysis focused on pressure loss, a key parameter affecting fluid resistance and energy consumption. Simulations show that increased layers in filters cause higher pressure losses, reflecting higher flow resistance. These findings align with the literature [75], suggesting that while increased thickness enhances particle capture efficiency, it also raises the energy required to maintain flow rates.

Pressure drops increase with flow and number of layers in both configurations. For Configuration A, the increase is 2 orders of magnitude for 4-layer filters (0.1–1000 ml/min), with a 40 % increase between 1 and 4 layers at 1000 ml/min. This configuration shows lower pressure losses than Configuration B (approximately 10 Pa, 170 Pa, and 315 Pa for the 1, 2, and 4-layers options, respectively). For Configuration B, losses increase by 1 order of magnitude with 1 layer and 3 orders with 4 layers in the same flow range, reflecting higher resistance, especially for thicker filters.

Then comparing the two configurations, Configuration B shows significantly higher pressure losses than Configuration A, with values approximately an order of magnitude higher at a maximum flow of 1000 ml/min and 4 layers. This indicates that the design of Configuration A may offer potentially lower energy consumption under high-flow conditions, particularly when thicker filters are used, due to a more efficient and less turbulent fluid path favored by its geometry. Configuration B, on the other hand, generates more turbulence and resistance, especially with thicker filters, while Configuration A facilitates smoother flow transitions by reducing the increase in pressure drop associated with the additional layers.

Analysis of flow velocity patterns showed how design affects fluid dynamics in filters. The velocity patterns were analyzed in both 2D and 3D across the filter's cross-sections, capturing the fluid distribution at different operating conditions. Fig. 2. A illustrates the 2D velocity profiles at the outlet of the simulated filter configuration, reported for all the modelled filters thickness, for the study case with an inlet flow rate of 10 ml/min. It offers a representative example of the flow distribution observed across various flow rates, trajectories, and its velocity along these paths. In Configuration A, increasing thickness progressively concentrates the flow velocity at the center of the filter, suggesting that the geometric design favors a centralized fluid path. In Configuration B, on the other hand, the velocity distribution remains uniform, even with thicker filters, indicating a more balanced approach and stable performance due to the internal design. Particle tracking simulations showed how the design affects retention, trajectories, and particle interaction with surfaces, providing a detailed picture of the performance of the two models. (Fig. 2B)

Configuration A favors stable, linear particle trajectories with constant velocities and minimal turbulence, reducing the risk of clogging and providing predictable performance for applications requiring controlled filtration. In contrast, Configuration B generates more complex trajectories, with turbulence and frequent interactions with the filter walls, increasing particle capture opportunities but leading to higher pressure losses and energy consumption, especially in multi-layer configurations (Figure S1). The analysis highlights how the choice of filter design must balance the needs of efficiency, energy consumption, and maintenance, taking advantage of the versatility of 3D printing to customize configurations, diameters, and layers to suit specific applications.

Therefore, the two structures were 3D printed by DLP. Printing parameters were optimized for each formulation, starting from previous work, and are shown in Table 1. Filter-type structures were successfully printed using the Asiga 3D-DLP printer and are shown in Fig. 1E and F. Printed structures exhibit flat surfaces, straight elements, and appear clean and sharp.

The use of a 3D scanner allowed us to assess print fidelity by creating a colorimetric map (Fig. 1G). Green denotes zero differences between the CAD model and the printed object, while red and blue represent positive or negative differences, respectively.

Surface functionalization of the specimens was achieved through reaction between amine groups and the reactive functional groups of the printed parts (epoxy, carboxylic and acrylate groups), as shown in Fig. 3. The nucleophilic attack of the N-electron pair of amines to an electron-deficient carbon atom is largely described and it does not need a

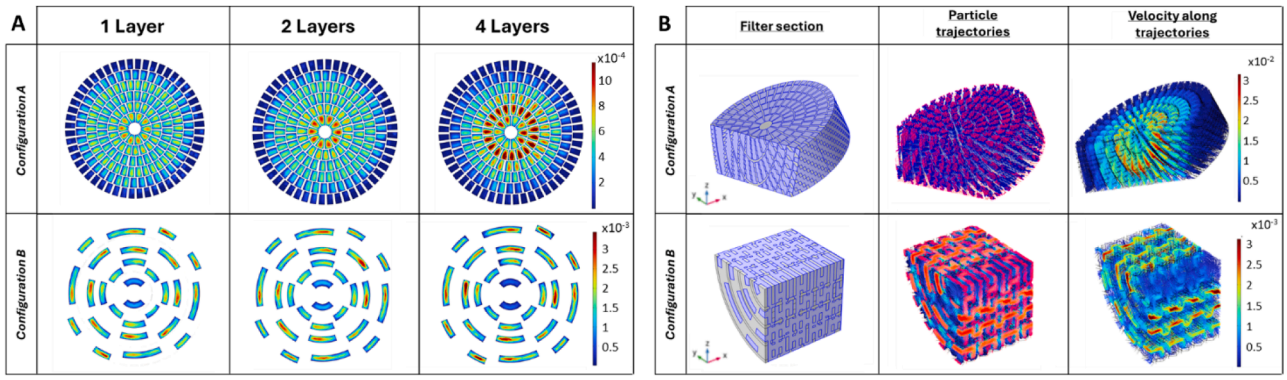


Fig. 2. 2D velocity trends at the filter outlet with an inlet flow rate of 10ml/min (A); 3D plot of filter cross section, trends of particle trajectories and particle velocities along the trajectories for configurations A and B (*B*).

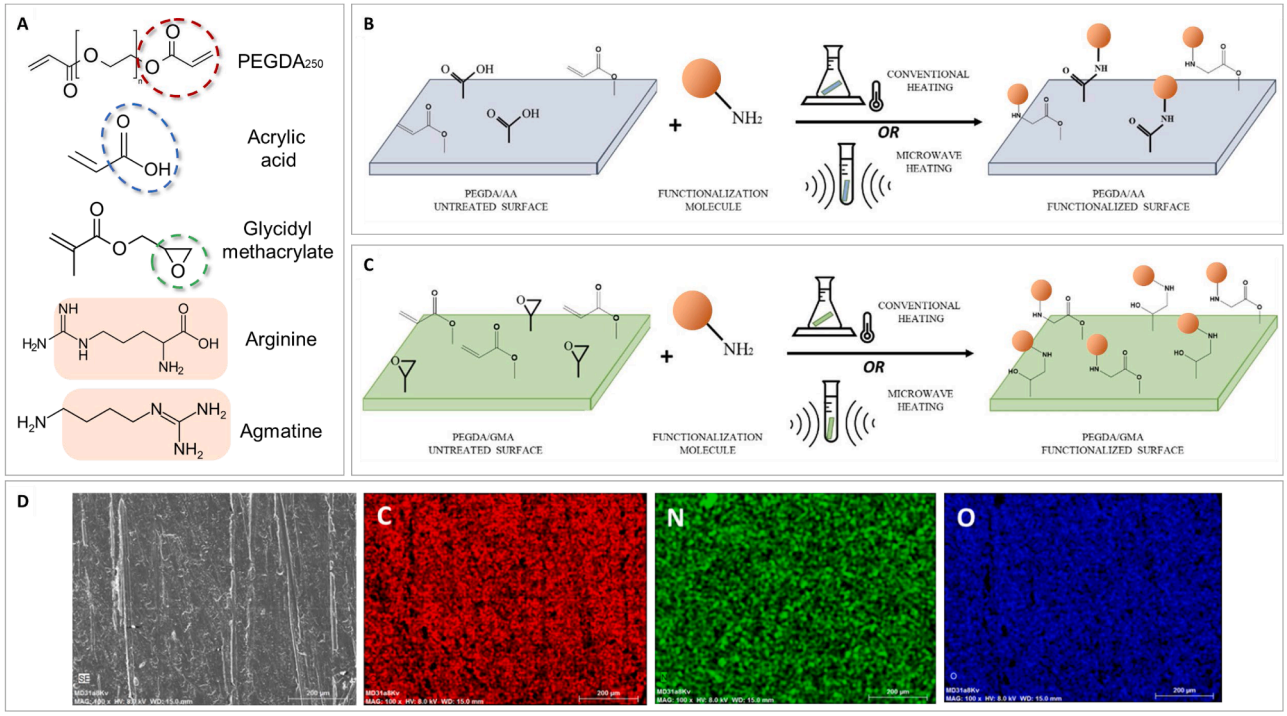


Fig. 3. – Chemical structure of PEGDA, Acrylic acid, glycidyl methacrylate, arginine and agmatine; functional groups of monomers are highlighted (acrylic group of PEGDA, in red; carboxyl group of acrylic acid, in blue; epoxy ring of glycidyl methacrylate, in green) (A); scheme of the surface functionalization procedure on 3D printed PEGDA/AA-based samples (B) and PEGDA/GMA-based samples (C). Different reactions take place, depending on the matrix: Michael addition to double bonds, that involves all matrices, amidation of the carboxylic group in PEGDA/AA matrix and epoxide group ring opening in PEGDA/GMA matrix. SEM image and EDX map of Carbon, Nitrogen and Oxygen distribution, for PAA-AG-C sample, showing the uniform distribution of the elements on the functionalized surface(D).

particular activation step [76]. For the amidation reaction of the acrylic acid group, we used EDC/NHS as coupling agents is widely described in the literature [77–79].

Conventionally, chemical reactions are thermally activated, and they are carried out through conductive heating, employing an external heat source in a liquid medium with grafting agents. As said before, this method, while effective, is slow and energy-consuming [73], due to dependence on convection currents and thermal conductivity [72].

As an alternative, microwave heating has been proven to be faster and more efficient [74], reducing byproduct formation [72] and thus increasing the yield [80]. This is due to a combination of two factors: the different way of transferring heat to the reagents and solvent and some specific activating (nonthermal) effects.

To identify the most effective functionalization conditions for each matrix–molecule pair, the reaction parameters, specifically reaction time and pH of the solution, were optimized using a dual-criteria approach. On the one hand, ATR-FTIR spectroscopy was employed to monitor the presence and the intensity of characteristic bands related to successful molecule incorporation. On the other hand, a sustainability-driven criterion was adopted, aiming to maximize surface functionalization while minimizing reaction time, thereby reducing energy consumption and processing time. The selection of the best reaction conditions was based on a combination of quantitative and qualitative criteria, derived from different characterization techniques.

Regarding ATR-FTIR spectroscopy, functionalization was considered successful when a clear increase in the intensity of bands at 1633 cm^{-1} and 1672 cm^{-1}, associated with guanidinium groups (from arginine and agmatine) [81], was observed. A simultaneous decrease in the 810 cm^{-1} band (C–H out-of-plane deformation of acrylate double bonds [82,83]) confirmed the occurrence of a reaction between acrylate and amine

groups. Additionally, in PEGDA/GMA-based samples, a decrease in the 905 cm^{-1} band signaled the opening of epoxy rings due to nucleophilic attack by the amines [84]. Other significative bands are in the 2870–2920 cm^{-1} and 3350–3450 cm^{-1} range, related to C—H symmetric stretching of aliphatic carbons [85] and N–H stretching vibration of secondary amines [86], respectively, that should increase with the surface functionalization. Only conditions that achieved these spectral features within the shortest reaction time possible and at a pH that ensured reproducibility and minimal degradation of the sample were selected as optimal. Results for each analyzed reaction time are in Figure S2, and the spectra of the optimized reactions are in Figure S3 and S4. The best reaction parameters are summarized in Table 3.

Complementary characterization techniques further supported the FTIR-based findings. EDX analysis was conducted to chemically characterize the samples' surface by measuring the weight percentage of nitrogen. Results are reported in Table 4, that shows increases in nitrogen content (≥3.0 wt%) on the surface of modified samples, with a homogeneous elemental distribution (Fig. 3D). The results for PEGDA/AA modification reactions show that the extent of the surface functionalization is very similar via conventional or MW heating, because of the same nitrogen content found by EDX technique. Although FTIR spectra indicate a slightly higher conversion than EDX under conventional heating, this discrepancy can be attributed to the different penetration depths of the two techniques. The ATR-FTIR beam typically probes a few micrometers into the material, whereas EDX rarely penetrates beyond 1 $^{\mu m}$ [87,88]. Since the materials are intended for surface-contact-killing antimicrobial applications, the surface-sensitive information provided by EDX is more relevant for evaluating the actual degree of surface modification.

Contact angle measurements indicated that most functionalized samples became more hydrophilic, particularly those based on PEGDA/AA. Exceptions were observed, such as the PGMA-AR-C sample, which showed increased hydrophobicity. These results are detailed in Table S3. Despite differences in surface wettability, PEGDA/AA-based samples showed greater swelling than PEGDA/GMA-based ones, due to their intrinsically more hydrophilic nature. Swelling behavior was not significantly influenced by the molecule used or the heating method, as shown in Table S3. Finally, TGA analysis (Figure S5) confirmed that functionalization had limited impact on the thermal stability of most samples, with degradation profiles comparable to untreated materials. However, PEGDA/AA samples treated with arginine displayed a distinct degradation pattern, with a main thermal event at 380 °C, potentially indicating structural changes induced by surface modification. Additional minor degradation events may reflect the decomposition of grafted amine groups and subsequent matrix degradation.

Having assessed the materials characteristics, anti-bacterial tests were conducted with both Gram-positive (*S. aureus*) and Gram-negative (*E. coli*) bacteria. Briefly, the inoculum was left to proliferate over the surfaces for 24 h and the viability of the adhered bacteria at the film surface was evaluated using a LIVE/DEAD fluorometric staining. Results of all bacterial tests are shown in Figures S6.

PEGDA/GMA-AG matrices showed the best antibacterial behavior, as can be observed in Fig. 4, which shows live (green) and dead (red) bacteria over PEGDA/GMA flat surfaces and PEGDA/GMA-AG samples modified via conventional or microwave functionalization. Both for *S. aureus* (Fig 4A) and *E. coli* (Fig 4B), viable bacteria colonies were observed over control PEGDA/GMA surfaces, with few to no dead bacteria attached. Interestingly, when AG was present, both after conventional and microwave functionalization, the number of dead bacteria becomes higher, evidencing the antimicrobial efficacy of this surface functionalization. This antimicrobial behavior has been further quantified via ImageJ software analysis: in all modified samples the percentage of area occupied by dead bacteria, both *S. aureus* (Fig 4C) and *E. coli* (Fig 4D), was found to be statistically significantly higher than the percentage of area occupied by live bacteria, also when compared to the respective controls.

As for the rest of the matrices, the antimicrobial behavior could not be quantified due to poor bacterial adhesion. It is possible that surface properties, such as charge and pH, influence bacterial adhesion, which is crucial for early-stage biofilm formation. Moreover, both specific and non-specific interactions may play an important role in the ability of the bacteria to attach to a biomaterial surface. The relative contributions of specific and nonspecific mechanisms are likely to depend on the surface properties of the biomaterial as well as the associated flow conditions [89]. In this case, the poor initial bacterial adhesion, which is essential for biofilm formation, could be influenced by the pH value in the culture environment and in the surface of the flat surfaces. In addition, the pH value could affect the surface charge of the matrices, since the Arginine and Agmatine residues can be protonated in different environments, leading to different conformational regimes of the surface [90]. Positively charged surfaces are supposed to be more adhesive, but the strong electrostatic attraction of the organisms has also been reported to impede surface growth of bacteria [91]. Nevertheless, the performed assay confirmed the antimicrobial efficacy of the modification herein described.

Discussion and conclusions

In this work, air filters with antibacterial properties were fabricated by 3D printing. In the first part, the design of the filters was studied, and different CAD geometries were designed, with the aim of maximizing the air/filter contact time and surface area. The two chosen configurations, A and B, have different characteristics: configuration A has greater mechanical stability, but allows only axial flow, while configuration B is also effective for radial air flows.

3D printing by DLP resulted in objects of high geometric complexity with high resolution, good mechanical properties and good fidelity to the original CAD model. While printing process with PEGDA/AA matrix was smoother, PEGDA/GMA required the presence of a dye to obtain an acceptable resolution, increasing the printing time.

Then, sample surfaces were successfully functionalized to give them bacterial adhesion characteristics. Two different molecules (arginine and agmatine) and two grafting functionalization techniques (by conventional and microwave heating) were used. As expected, microwave heating gave a degree of functionalization comparable to the one given by conventional heating, with much less time needed and thus less energy consumption. The decrease in reaction time needed for obtaining the same degree of functionalization is around a factor of 120 for all reactions. All those findings were supported by FT-IR spectroscopy, which clearly showed the presence of peaks that can be associated to the

Table 4
– Element percentage (wt%) on samples' surface.

	PEGDA/AA					PEGDA/GMA				
Element	Untreated	AR-C	AR-M	AG-C	AG-M	Untreated	AR-C	AR-M	AG-C	AG-M
C	52.46	53.10	52.74	52.60	52.79	56.92	52.24	n.a.	52.37	54.26
O	44.87	43.06	43.49	41.38	41.56	41.23	43.32	n.a.	43.09	44.25
N	0.44	1.29	3.06	3.25	3.66	1.85	3.04	n.a.	2.68	0.27
Others	2.23	2.55	0.71	2.77	1.99	0	1.4	n.a.	1.86	1.22
Total	100	100	100	100	100	100	100	—	100	100

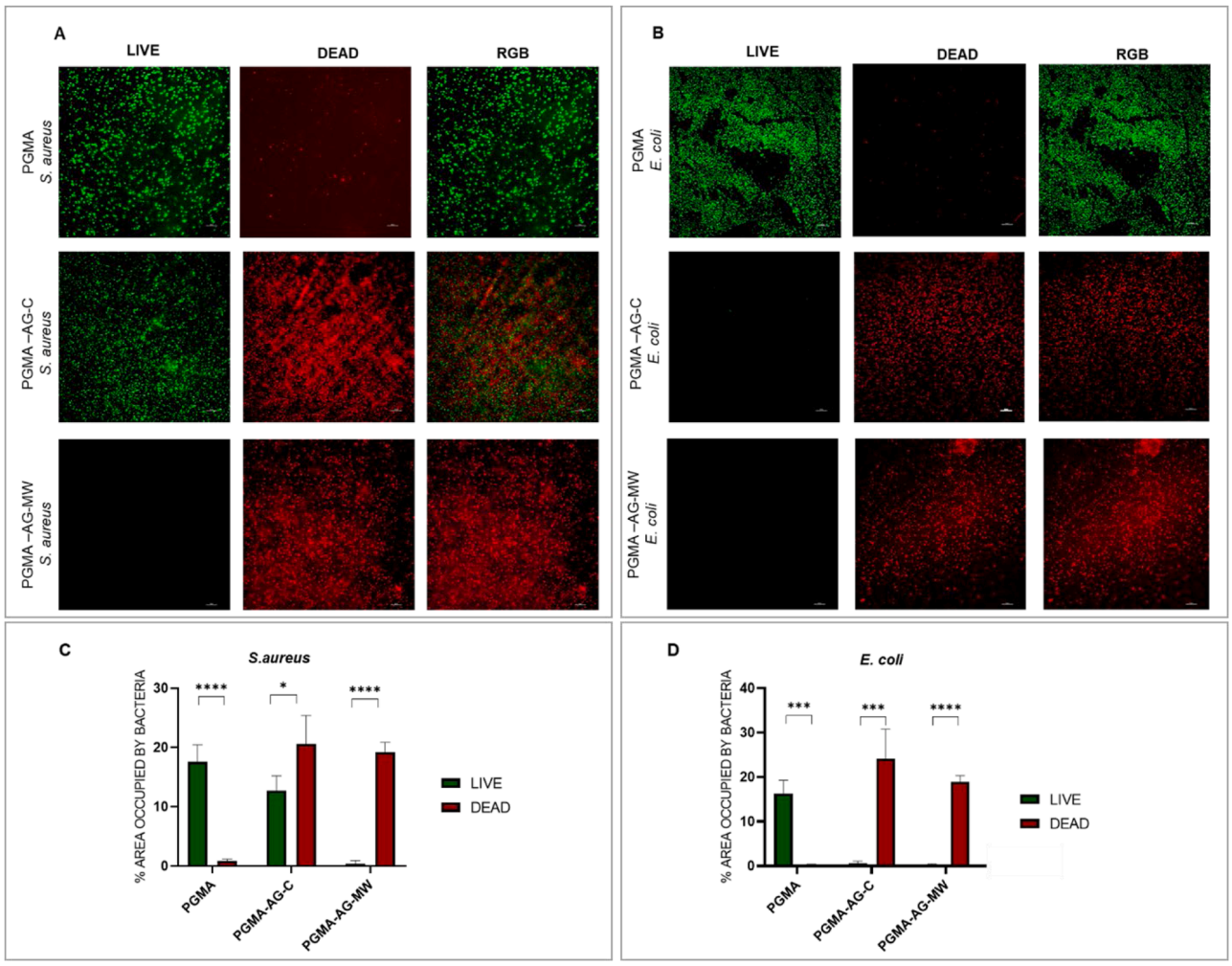


Fig. 4. LIVE/DEAD assay for PEGDA/GMA flat surfaces. Micrographies of S. aureus bacteria stained over the sample surfaces (scale bar is 20 μm) (A). Micrographies of *E. coli* bacteria stained over the sample surfaces (scale bar is 20 μm) (B). Surface area coverage (%) of bacteria culture after ImageJ analysis for S. aureus (C); Surface area coverage (%) of bacteria culture after ImageJ analysis for *E. coli* (D). Experiment was conducted in triplicate and statistical analysis was performed with two-ways ANOVA (* $p < 0.05$, ** $p < 0.01$, *** $p < 0.001$, ****$p < 0.0001$).

functionalization. These results, together with the use of natural amino acids and aqueous buffers, makes functionalization through microwave heating a sustainable way to give antibacterial properties.

Chemical modification is witnessed also by changes in surface and thermal properties. With respect to the variation of hydrophilicity, a certain spread of contact angle values was measured, nevertheless all are within an adequate range of wettability in which the interaction with bacteria and the adhesion process is favored [92]. Related to thermal properties, TGA experiments show limited changes of the thermogram, suggesting that only the surface was chemically modified, without strong modifications of bulk properties. Besides, the presence of new degradation peaks confirms the successful modification.

Reproducibility was ensured by applying standardized protocols, repeated measurements and the use of complementary characterization techniques (FTIR, EDX, contact angle). Statistical analysis of the data and comparison between replicates confirmed the reliability of the observed trends, while recognizing that minor fluctuations are inevitable in these systems, due to the inherent heterogeneity of 3D printing and surface functionalization processes.

Regarding bacterial adhesion, samples were tested with Gram-positive and Gram-negative bacteria. The antimicrobial efficacy of the modification has been proved in the PEGDA/GMA-AG surfaces, which showed a higher number of dead bacteria attached to the surface, both after conventional and microwave functionalization. Particularly, the microwave functionalized filters exhibited the most consistent antimicrobial behavior in the inactivation of both bacterial strains tested, proving to be to be a faster and more efficient way to achieve the desired effectiveness within our antimicrobial strategy.

Also, the theoretical effectiveness of the filters in application scenarios was studied through flow simulations, where filters are placed inside ducts with a water flow, showing that Configuration A is more balanced and less energy demanding, while Configuration B optimizes particle retention but with greater pressure losses, energy consumption and risk of clogging, especially in multi-layer systems.

Numerical results obtained from CFD simulations provide valuable support for predicting filter behavior and performance in a realistic application context, pointing out some indicative correlations between geometry, flow distribution and antibacterial performance. Simulations show that Configuration A favors a central and linear flow, with less turbulence and wall interaction, which could translate into a lower probability of bacterial accumulation and, therefore, a more controlled environment for filtration. Configuration B, in contrast, has more turbulent trajectories and more frequent interactions with filter surfaces, which may increase capture efficiency but also increase the risk of bacterial occlusion or proliferation in the absence of functionalized surfaces. In this context, the antibacterial efficacy of PEGDA/GMA-AG surfaces, evidenced by the significant presence of dead bacteria, can be read as a complementary strategy to the use of a flow-friendly

geometry (as in Configuration A), in order to balance filtration efficiency, filter life and microbiological safety.

The use of CAD models and 3D printing offers significant advantages in terms of dimensional and process scalability. The ability to quickly adapt digital design enables the production of components in different sizes without additional tooling costs. Furthermore, with the possibilities of 3D printing, multiple components can be produced at the same time, saving time and making it easy to scale. This flexibility in design and production encourages amid rapid prototyping and on-demand production, which reduces waste, development time, and overall cost. Additionally, the investigated geometries can be readily scaled in terms of thickness—by choosing the correct number of layers—and diameter, allowing for fine-tuning of the final dimensions to match specific applications' needs. This scalability makes it possible to adapt the same design to different functional needs without re-engineering the entire component. Additionally, thermosets such as acrylic polymers are well-known for their long-term stability in standard conditions. In this case this is demonstrated observing that the surface integrity and the original geometries were preserved throughout the process. Additionally, the antibacterial tests were carried out several weeks after the functionalization procedures. During this time, no structural changes or deterioration were observed, which suggests a good level of stability over time under ambient storage conditions. On the other hand, applications in harsh conditions (i.e. high temperatures, pressures or extreme pHs) should be instead checked specifically, since degradation of the polymers may occur.

Summarizing, 3D printing complex geometries were fabricated, and surface functionalized to give antimicrobial properties. Having determined the best conditions, in the next future new studies will be developed to these prototypes, to verify the efficacy of these devices.

CRediT authorship contribution statement

Maria D'Aloia: Writing – original draft, Investigation. **Raquel Cue López:** Writing – review & editing, Investigation. **Simona Villata:** Writing – review & editing, Investigation. **Nicolò Santi Vasile:** Writing – review & editing, Investigation. **Enrique Martínez Campos:** Writing – review & editing, Resources. **Laura Montalvillo Jiménez:** Investigation. **Candido Fabrizio Pirri:** Writing – review & editing, Funding acquisition. **Francesca Frascella:** Writing – review & editing, Resources, Conceptualization. **Paula Bosch:** Writing – review & editing, Supervision, Methodology. **Ignazio Roppolo:** Writing – original draft, Supervision, Methodology, Conceptualization.

Declaration of competing interest

The authors declare the following financial interests/personal relationships which may be considered as potential competing interests:

Francesca Frascella reports financial support was provided by Ministry of University and Research. Paula Bosch reports financial support was provided by European Union. Paula Bosch reports financial support was provided by CSIC Interdisciplinary Thematic Platform. If there are other authors, they declare that they have no known competing financial interests or personal relationships that could have appeared to influence the work reported in this paper.

Funding

This work was supported by the National Plan for Complementary Investments to the NRRP, project "D34H—Digital Driven Diagnostics, prognostics and therapeutics for sustainable Health care" (project code: PNC0000001), Spoke 4 funded by the Italian Ministry of University and Research. This work was also funded by European Union (Nextgeneration EU) and CSIC Interdisciplinary Thematic Platform Salud Global+ (PTI-SALUDGLOBAL+).

Supplementary materials

Supplementary material associated with this article can be found, in the online version, at doi:10.1016/j.apmt.2025.102779.

Data availability

Data will be made available on request.

References

[1] T. Lu, J. Cui, Q. Qu, Y. Wang, J. Zhang, R. Xiong, W. Ma, C. Huang, Multistructured electrospun nanofibers for air filtration: a review, ACS. Appl. Mater. Interfaces. 13 (2021).
[2] C. Yang, Aerosol filtration application using fibrous Media - an industrial perspective, Chin. J. Chem. Eng. 20 (2012), https://doi.org/10.1016/S1004-9541(12)60356-5.
[3] M. Zhu, J. Han, F. Wang, W. Shao, R. Xiong, Q. Zhang, H. Pan, Y. Yang, S.K. Samal, F. Zhang, et al., Electrospun nanofibers membranes for effective air filtration, Macromol. Mater. Eng. 302 (2017).
[4] S. Peron, R. Pancholi, B. Voelcker, J.D. Wittenbach, H.F. Ólafsdóttir, J. Freeman, K. Svoboda, Recurrent interactions in local cortical circuits, Nature 579 (2020), https://doi.org/10.1038/s41586-020-2062-x.
[5] C.J.E. Metcalf, J. Lessler, Opportunities and challenges in modeling emerging infectious diseases, Science (1979) 357 (2017).
[6] W.W.F. Leung, Q. Sun, Charged PVDF multilayer nanofiber filter in filtering simulated airborne novel coronavirus (COVID-19) using ambient nano-aerosols, Sep. Purif. Technol. 245 (2020), https://doi.org/10.1016/j.seppur.2020.116887.
[7] W.N. Harrington, C.M. Kackos, R.J. Webby, The evolution and future of Influenza Pandemic preparedness, Exp. Mol. Med. 53 (2021).
[8] T. Bourdrel, M.A. Bind, Y. Béjot, O. Morel, J.F. Argacha, Cardiovascular effects of air pollution, Arch. Cardiovasc. Dis. 110 (2017).
[9] Q. Zhang, X. Jiang, D. Tong, S.J. Davis, H. Zhao, G. Geng, T. Feng, B. Zheng, Z. Lu, D.G. Streets, et al., Transboundary health impacts of transported global air pollution and international trade, Nature 543 (2017), https://doi.org/10.1038/nature21712.
[10] A. Sabirova, S. Wang, G. Falca, P.Y. Hong, S.P. Nunes, Flexible isoporous air filters for high-efficiency particle capture, Polymer. (Guildf) 213 (2021), https://doi.org/10.1016/j.polymer.2020.123278.
[11] D.W. Wei, H. Wei, A.C. Gauthier, J. Song, Y. Jin, H. Xiao, Superhydrophobic modification of cellulose and cotton textiles: methodologies and applications, J. Biores. Bioprod. 5 (2020).
[12] G. Liu, M. Xiao, X. Zhang, C. Gal, X. Chen, L. Liu, S. Pan, J. Wu, L. Tang, D. Clements-Croome, A review of air filtration technologies for sustainable and healthy building ventilation, Sustain. Cities. Soc. 32 (2017).
[13] L.M. Henning, A. Abdullayev, C. Vakifahmetoglu, U. Simon, H. Bensalah, A. Gurlo, M.F. Bekheet, Review on polymeric, inorganic, and composite materials for air filters: from processing to properties, Adv. Energy Sustainab. Res. 2 (2021).
[14] S. Lee, A.R. Cho, D. Park, J.K. Kim, K.S. Han, I.J. Yoon, M.H. Lee, J. Nah, Reusable polybenzimidazole nanofiber membrane filter for highly breathable PM 2.5 dust proof mask, ACS. Appl. Mater. Interfaces. 11 (2019), https://doi.org/10.1021/acsami.8b19741.
[15] Y. Zhang, Z. Zeng, X.Y.D. Ma, C. Zhao, J.M. Ang, B.F. Ng, M.P. Wan, S.C. Wong, Z. Wang, X. Lu, Mussel-inspired approach to cross-linked functional 3D nanofibrous aerogels for energy-efficient filtration of ultrafine airborne particles, Appl. Surf. Sci. 479 (2019), https://doi.org/10.1016/j.apsusc.2019.02.173.
[16] R. Roche, F. Yalcinkaya, Electrospun polyacrylonitrile nanofibrous membranes for point-of-use water and air cleaning, ChemistryOpen. 8 (2019), https://doi.org/10.1002/open.201800267.
[17] Z. Jiang, H. Zhang, M. Zhu, D. Lv, J. Yao, R. Xiong, C. Huang, Electrospun soy-protein-based nanofibrous membranes for effective antimicrobial air filtration, J. Appl. Polym. Sci. 135 (2018), https://doi.org/10.1002/app.45766.
[18] A.C.C. Bortolassi, S. Nagarajan, B. de Araújo Lima, V.G. Guerra, M.L. Aguiar, V. Huon, L. Soussan, D. Cornu, P. Miele, M. Bechelany, Efficient nanoparticles removal and bactericidal action of electrospun nanofibers membranes for air filtration, Mater. Sci. Eng. C 102 (2019), https://doi.org/10.1016/j.msec.2019.04.094.
[19] H. He, M. Gao, B. Illés, K. Molnar, 3D Printed and electrospun, transparent, hierarchical polylactic acid mask nanoporous filter, Int. J. Bioprint. 6 (2020), https://doi.org/10.18063/ijb.v6i4.278.
[20] M. Ali, A. Qura Tul, Advances In air filters based on electrospun nanofibers, Environ. Contamin. Rev. (ECR) 3 (2020) 32–36.
[21] K. Sathish, S.S. Kumar, R.T. Magal, V. Selvaraj, V. Narasimharaj, R. Karthikeyan, G. Sabarinathan, M. Tiwari, A.E. Kassa, A comparative study on subtractive manufacturing and additive manufacturing, Adv. Mater. Sci. Eng. 2022 (2022).
[22] M.A. Kreiger, M.L. Mulder, A.G. Glover, J.M. Pearce, Life cycle analysis of distributed recycling of post-consumer high density polyethylene for 3-D printing filament, J. Clean. Prod. 70 (2014), https://doi.org/10.1016/j.jclepro.2014.02.009.
[23] H. Paris, H. Mokhtarian, E. Coatanéa, M. Museau, I.F. Ituarte, Comparative environmental impacts of additive and subtractive manufacturing technologies, CIRP. Ann. Manuf. Technol. 65 (2016), https://doi.org/10.1016/j.cirp.2016.04.036.

[24] X. Xu, S. Xiao, H.J. Willy, T. Xiong, R. Borayek, W. Chen, D. Zhang, J. Ding, 3D-Printed grids with polymeric photocatalytic system as flexible air filter, Appl. Catal. B 262 (2020), https://doi.org/10.1016/j.apcatb.2019.118307.
[25] M. Javaid, A. Haleem, R.P. Singh, R. Suman, S. Rab, Role of additive manufacturing applications towards environmental sustainability, Adv. Industr. Eng. Polym. Res. 4 (2021).
[26] E. Mathew, B.F. Gilmore, E. Larrañeta, D.A. Lamprou, Antimicrobial 3D printed objects in the fight against pandemics, 3D. Print. Addit. Manuf. 8 (2021).
[27] Y. Wang, F. Wang, H. Zhang, B. Yu, H. Cong, Y. Shen, Antibacterial material surfaces/interfaces for biomedical applications, Appl. Mater. Today 25 (2021), https://doi.org/10.1016/j.apmt.2021.101192.
[28] Y. Liu, Q. Zhao, Influence of surface energy of modified surfaces on bacterial adhesion, Biophys. Chem. 117 (2005), https://doi.org/10.1016/j.bpc.2005.04.015.
[29] J. Hasan, R.J. Crawford, E.P. Ivanova, Antibacterial surfaces: the quest for a new generation of biomaterials, Trends Biotechnol. 31 (2013).
[30] A. Arora, A. Mishra, Antibacterial polymers - A mini review, in: Proceedings of the Materials Today: Proceedings 5, 2018.
[31] N. Nasri, A. Rusli, N. Teramoto, M. Jaafar, K.M.K. Ishak, M.D. Shafiq, Z.A. A. Hamid, Past and current progress in the development of antiviral/antimicrobial polymer coating towards covid-19 prevention: a review, Polymers. (Basel) 13 (2021).
[32] J. Lei, L.C. Sun, S. Huang, C. Zhu, P. Li, J. He, V. Mackey, D.H. Coy, Q.Y. He, The antimicrobial peptides and their potential clinical applications, Am. J. Transl. Res. 11 (2019).
[33] A.W. McFarland, A. Elumalai, C.C. Miller, A. Humayun, D.K. Mills, Effectiveness and applications of a metal-coated HNT/polylactic acid antimicrobial filtration system, Polymers. (Basel) 14 (2022), https://doi.org/10.3390/polym14081603.
[34] A.C. Ogazi, P.O. Osifo, Inhibition of coliforms and *Escherichia coli* bacterial strains in water by 3D printed CS/GO/AgNP filtration membranes, J. Polym. Environ. 31 (2023), https://doi.org/10.1007/s10924-023-02889-9.
[35] B. Thavornyutikarn, T. Lertwimol, W. Kosorn, W. Hankamolsiri, N. Nampichai, W. Janvikul, 3D-Printing antibacterial composite Filaments containingsynergistic antibacterial activity of green tea and tannic acid, Polym. Adv. Technol. 32 (2021) 4733–4744.
[36] A.C. Lehnen, S. Hanke, M. Schneider, C.M.L. Radelof, J. Perestrelo, S. Reinicke, M. Reifarth, A. Taubert, K.M. Arndt, M. Hartlieb, Modification of 3D-printed PLA structures using photo-iniferter polymerization: toward on-demand antimicrobial water filters, Macromol. Rapid. Commun. 44 (2023), https://doi.org/10.1002/marc.202300408.
[37] G. Gonzalez, A. Chiappone, K. Dietliker, C.F. Pirri, I. Roppolo, Fabrication and functionalization of 3D printed polydimethylsiloxane-based microfluidic devices obtained through digital light processing, Adv. Mater. Technol. 5 (2020), https://doi.org/10.1002/admt.202000374.
[38] Z. Zhi, T. Xiaoxiao, S. Xiaoyan, Engineering materials with light: recent progresses in digital light processind based 3D printing, J. Mater. Chem. C. Mater. 8 (2020) 13896–13917.
[39] M. Layani, X. Wang, S. Magdassi, Novel materials for 3D printing by photopolymerization, Adv. Mater. 30 (2018).
[40] M. Caprioli, I. Roppolo, A. Chiappone, L. Larush, C.F. Pirri, S. Magdassi, 3D-Printed self-healing hydrogels via digital light processing, Nat. Commun. 12 (2021), https://doi.org/10.1038/s41467-021-22802-z.
[41] D. Cvetković (Ed.), 3D Printing, InTech, 2018. Ed.
[42] T. Norton, D.W. Sun, Computational fluid dynamics (CFD) - an effective and efficient design and analysis tool for the food industry: a review, Trends. Food Sci. Technol. 17 (2006).
[43] M. Rebaï, M. Prat, M. Meireles, P. Schmitz, R. Baclet, A semi-analytical model for gas flow in pleated filters, Chem. Eng. Sci. 65 (2010), https://doi.org/10.1016/j.ces.2010.01.014.
[44] S. Fotovati, S.A. Hosseini, H. Vahedi Tafreshi, B. Pourdeyhimi, Modeling instantaneous pressure drop of pleated thin filter Media during dust loading, Chem. Eng. Sci. 66 (2011), https://doi.org/10.1016/j.ces.2011.05.038.
[45] Z. Feng, Z. Long, Q. Chen, Assessment of various CFD models for predicting airflow and pressure drop through pleated filter system, Build. Environ. 75 (2014), https://doi.org/10.1016/j.buildenv.2014.01.022.
[46] A. Iranzo, CFD Applications in Energy engineering research and Simulation: an introduction to published reviews, Processes 7 (2019), https://doi.org/10.3390/pr7120883.
[47] J. Tu, G.H. Yeoh, C. Liu, Computat. Fluid Dyn. (2018).
[48] D.S. Jarman, M.G. Faram, G. Tabor, D. Butler, A review of the opportunities presented through the application of computational fluid dynamics (CFD) to water management challenges, in: Proceedings of the Proceedings of the Combined International Conference of Computing and Control for the Water Industry, CCWI2007 and Sustainable Urban Water Management, 2007. SUWM2007.
[49] M. Gastaldi, F. Cardano, M. Zanetti, G. Viscardi, C. Barolo, S. Bordiga, S. Magdassi, A. Fin, I. Roppolo, Functional dyes in polymeric 3D printing: applications and perspectives, ACS. Mater. Lett. 3 (2021).
[50] G. Gonzalez, I. Roppolo, C.F. Pirri, A. Chiappone, Current and emerging trends in polymeric 3D printed microfluidic devices, Addit. Manuf. 55 (2022).
[51] X. Meng, R. Xing, S. Liu, H. Yu, K. Li, Y. Qin, P. Li, Molecular weight and PH effects of aminoethyl modified chitosan on antibacterial activity in vitro, Int. J. Biol. Macromol. 50 (2012), https://doi.org/10.1016/j.ijbiomac.2012.01.018.
[52] K.A. Gibney, I. Sovadinova, A.I. Lopez, M. Urban, Z. Ridgway, G.A. Caputo, K. Kuroda, Poly(Ethylene Imine)s as antimicrobial agents with selective activity, Macromol. Biosci. 12 (2012), https://doi.org/10.1002/mabi.201200052.
[53] Y. Qian, S. Deng, Z. Cong, H. Zhang, Z. Lu, N. Shao, S.A. Bhatti, C. Zhou, J. Cheng, S.H. Gellman, et al., Secondary Amine pendant β-peptide polymers displaying potent antibacterial activity and promising therapeutic potential in treating MRSA-induced wound infections and keratitis, J. Am. Chem. Soc. 144 (2022), https://doi.org/10.1021/jacs.1c10659.
[54] S.E. Exley, L.C. Paslay, G.S. Sahukhal, B.A. Abel, T.D. Brown, C.L. McCormick, S. Heinhorst, V. Koul, V. Choudhary, M.O. Elasri, et al., Antimicrobial peptide mimicking primary amine and guanidine containing methacrylamide copolymers prepared by Raft polymerization, Biomacromolecules. 16 (2015), https://doi.org/10.1021/acs.biomac.5b01162.
[55] A. Nimmagadda, X. Liu, P. Teng, M. Su, Y. Li, Q. Qiao, N.K. Khadka, X. Sun, J. Pan, H. Xu, et al., Polycarbonates with potent and selective antimicrobial activity toward gram-positive bacteria, Biomacromolecules. 18 (2017), https://doi.org/10.1021/acs.biomac.6b01385.
[56] S.H. Kim, D. Semenya, D. Castagnolo, Antimicrobial drugs bearing guanidine moieties: a review, Eur. J. Med. Chem. 216 (2021).
[57] S. Sam, B. Joseph, S. Thomas, Exploring the antimicrobial features of biomaterials for biomedical applications, Results. Eng. 17 (2023), https://doi.org/10.1016/j.rineng.2023.100979.
[58] W. Raasch, S. Regunathan, G. Li, D.J.Agmatine Reis, the bacterial amine, is widely distributed in mammalian tissues, Life Sci. 56 (1995), https://doi.org/10.1016/0024-3205(95)00226-V.
[59] K.J. Cutrona, B.A. Kaufman, D.M. Figueroa, D.E. Elmore, Role of arginine and lysine in the antimicrobial mechanism of histone-derived antimicrobial peptides, FEBS Lett. 589 (2015), https://doi.org/10.1016/j.febslet.2015.11.002.
[60] M. Sepahi, R. Jalal, M. Mashreghi, Antibacterial activity of poly-L-arginine under different conditions, Iran. J. Microbiol. 9 (2017).
[61] K. Andreev, C. Bianchi, J.S. Laursen, L. Citterio, L. Hein-Kristensen, L. Gram, I. Kuzmenko, C.A. Olsen, D. Gidalevitz, Guanidino groups greatly enhance the action of antimicrobial peptidomimetics against bacterial cytoplasmic membranes, Biochim. Biophys. Acta Biomembr. 1838 (2014), https://doi.org/10.1016/j.bbamem.2014.05.022.
[62] N.W. Schmidt, K.P. Tai, K. Kamdar, A. Mishra, G.H. Lai, K. Zhao, A.J. Ouellette, G. C.L. Wong, Arginine in α-defensins: differential effects on bactericidal activity correspond to geometry of membrane curvature generation and peptide-lipid phase behavior, J. Biolog. Chem. 287 (2012), https://doi.org/10.1074/jbc.M112.358721.
[63] K.E.S. Locock, T.D. Michl, J.D.P. Valentin, K. Vasilev, J.D. Hayball, Y. Qu, A. Traven, H.J. Griesser, L. Meagher, M. Haeussler, Guanylated polymethacrylates: a class of potent antimicrobial polymers with low hemolytic activity, Biomacromolecules. 14 (2013), https://doi.org/10.1021/bm401128r.
[64] J. Svenson, R. Karstad, G.E. Flaten, B.O. Brandsdal, M. Brandl, J.S. Svendsen, Altered activity and physicochemical properties of short cationic antimicrobial peptides by incorporation of arginine analogues, Mol. Pharm. 6 (2009), https://doi.org/10.1021/mp900057k.
[65] M. Ginesy, J. Belotserkovsky, J. Enman, L. Isaksson, U. Rova, Metabolic engineering of *Escherichia coli* for enhanced arginine biosynthesis, Microb. Cell Fact. 14 (2015), https://doi.org/10.1186/s12934-015-0211-y.
[66] F. Galgano, M. Caruso, N. Condelli, F. Favati, Focused review: agmatine in Fermented foods, Front. Microbiol. 3 (2012), https://doi.org/10.3389/fmicb.2012.00199.
[67] T. Utagawa, Production of arginine by fermentation, in: Proceedings of the Journal of Nutrition 134, 2004.
[68] N. Rekowska, J. Huling, A. Brietzke, D. Arbeiter, T. Eickner, J. Konasch, A. Riess, R. Mau, H. Seitz, N. Grabow, et al., Thermal, mechanical and biocompatibility analyses of photochemically polymerized PEGDA250 for photopolymerization-based manufacturing processes, Pharmaceutics. 14 (2022), https://doi.org/10.3390/pharmaceutics14030628.
[69] S. Lantean, I. Roppolo, M. Sangermano, C.F. Pirri, A. Chiappone, Development of new hybrid acrylic/epoxy DLP-3D printable materials, Inventions 3 (2018), https://doi.org/10.3390/inventions3020029.
[70] K.A. Schug, W. Lindner, Noncovalent binding between guanidinium and anionic groups: focus on biological- and synthetic-based arginine/guanidinium interactions with phosph[on]ate and sulf[on]ate residues, Chem. Rev. 105 (2005).
[71] A. Kumar, Y. Kuang, Z. Liang, X. Sun, Microwave chemistry, recent advancements, and eco-friendly Microwave-assisted synthesis of nanoarchitectures and their applications: a review, Mater. Today Nano. 11 (2020).
[72] S. Das, A.K. Mukhopadhyay, S. Datta, D. Basu, Prospects of microwave processing: an overview, Bullet. Mater. Sci. 32 (2009).
[73] C.O. Kappe, D. Dallinger, S.S. Murphree, Pract. Microw. Synth. Organic Chem. (2008).
[74] A. Hou, X. Wang, L. Wu, Effect of microwave irradiation on the physical properties and morphological structures of cotton cellulose, Carbohydr. Polym. 74 (2008), https://doi.org/10.1016/j.carbpol.2008.05.011.
[75] B. Halder, A. Shukla, CFD Anal. Fluid Flow through U-Pipe 5 (2017).
[76] D.V. Mifsud, Z. Kaňuchová, P. Herczku, S. Ioppolo, Z. Juhász, S.T.S. Kovács, N. J. Mason, R.W. McCullough, B. Sulik, Sulfur ice astrochemistry: a review of Laboratory studies, Space Sci. Rev. 217 (2021).
[77] M.J.E. Fischer, Amine coupling through EDC/NHS: a practical approach, Methods Mol. Biol. 627 (2010), https://doi.org/10.1007/978-1-60761-670-2_3.
[78] E.Y. Liu, S. Jung, H. Yi, Improved protein conjugation with uniform, macroporous poly(Acrylamide-Co-Acrylic Acid) hydrogel microspheres via EDC/NHS chemistry, Langmuir. 32 (2016), https://doi.org/10.1021/acs.langmuir.6b02591.
[79] C. Wang, Q. Yan, H.B. Liu, X.H. Zhou, S.J. Xiao, Different EDC/NHS activation mechanisms between PAA and PMAA brushes and the following amidation reactions, Langmuir. 27 (2011), https://doi.org/10.1021/la202267p.

[80] G. Gonzalez, M. Arévalo, A. Chiappone, E. Martínez Campos, C.F. Pirri, I. Roppolo, P. Bosch, A facile and green microwave-assisted strategy to induce surface properties on complex-shape polymeric 3D printed structures, Macromol. Mater. Eng. 308 (2023), https://doi.org/10.1002/mame.202300118.
[81] A. Barth, The infrared absorption of amino acid side chains, Prog. Biophys. Mol. Biol. 74 (2000).
[82] S. Kaewpirom, D. Kunwong, Curing behavior and cured film performance of easy-to-clean UV-curable coatings based on hybrid urethane acrylate oligomers, J. Polymer Res. 19 (2012), https://doi.org/10.1007/s10965-012-9995-1.
[83] W.N.E. van Dijk-Wotthuis, O. Franssen, H. Talsma, M.J. van Steenbergen, J. J. Kettenes-van den Bosch, W.E. Hennink, Synthesis, characterization, and polymerization of glycidyl methacrylate derivatized dextran, Macromolecules. 28 (1995), https://doi.org/10.1021/ma00122a044.
[84] N. Flores-Ramírez, E.A. Elizalde-Peña, S.R. Vásquez-García, J. González-Hernández, A. Martinez-Ruvalcaba, I.C. Sanchez, G. Luna-Bárcenas, R.B. Gupta, Characterization and degradation of functionalized Chitosan with glycidyl methacrylate, J. Biomater. Sci. Polym. Ed. 16 (2005), https://doi.org/10.1163/1568562053700174.
[85] A. Bosch, D. Serra, C. Prieto, J. Schmitt, D. Naumann, O. Yantorno, Characterization of Bordetella Pertussis growing as biofilm by chemical analysis and FT-IR spectroscopy, Appl. Microbiol. Biotechnol. 71 (2006), https://doi.org/10.1007/s00253-005-0202-8.
[86] G. Theivandran, S.M. Ibrahim, M. Murugan, Fourier transform infrared (Ft-Ir) spectroscopic analysis of Spirulina Fusiformis, ~ 30 ~ J. Medic. Plants Stud. 3 (2015).
[87] H. Kaur, B. Rana, D. Tomar, S. Kaur, K.C. Jena, Fundamentals of ATR-FTIR spectroscopy and its role for probing In-situ molecular-level interactions, Progress Opt. Sci. Photon. 13 (2021).
[88] M. Abd Mutalib, M.A. Rahman, M.H.D. Othman, A.F. Ismail, J. Jaafar, Scanning electron microscopy (SEM) and energy-dispersive X-ray (EDX) spectroscopy, Membrane Characteriz. (2017).
[89] J.E. Klinth, M. Castelain, B.E. Uhlin, O. Axner, The influence of PH on the specific adhesion of P piliated *Escherichia coli*, PLoS. One 7 (2012), https://doi.org/10.1371/journal.pone.0038548.
[90] D.E.S. Santos, D. Li, M. Ramstedt, J.E. Gautrot, T.A. Soares, Conformational dynamics and responsiveness of weak and strong polyelectrolyte brushes: atomistic simulations of poly(Dimethyl Aminoethyl Methacrylate) and poly(2-(Methacryloyloxy)ethyl trimethylammonium chloride), Langmuir. 35 (2019), https://doi.org/10.1021/acs.langmuir.8b04268.
[91] B. Gottenbos, D.W. Grijpma, H.C. Van Der Mei, J. Feijen, H.J. Busscher, Antimicrobial effects of positively charged surfaces on adhering gram-positive and gram-negative bacteria, J. Antimicrob. Chemother. 48 (2001), https://doi.org/10.1093/jac/48.1.7.
[92] Y. Yuan, M.P. Hays, P.R. Hardwidge, J. Kim, Surface characteristics influencing bacterial adhesion to polymeric substrates, RSC. Adv. 7 (2017), https://doi.org/10.1039/c7ra01571b.